Miscible ferrofluid patterns in a radial magnetic field

Ching-Yao Chen,[1,*] Y.-S. Yang,[1] and José A. Miranda[2,†]
[1]*Department of Mechanical Engineering, National Chiao Tung University, Hsinchu, Taiwan 30010, Republic of China*
[2]*Departamento de Física, LFTC, Universidade Federal de Pernambuco, Recife 50670-901, PE, Brazil*
(Received 19 March 2009; revised manuscript received 29 April 2009; published 22 July 2009)

Pattern formation in a miscible ferrofluid system is experimentally investigated. The experiment is performed by immersing a thin ferrofluid droplet in a cylindrical container, overfilling it with a nonmagnetic miscible fluid, and applying an in-plane radial magnetic field. Visually striking patterns are obtained whose morphologies change from circular at zero field to complex starburstlike structures at finite field. The evolution of miscible ferrofluid droplets of various initial diameters subjected to different magnetic-field strengths is considered. Proper rescaling of the experimental data indicates that the time evolution of the droplets' area increments obeys a universal 4/3 power-law behavior at long times.

DOI: 10.1103/PhysRevE.80.016314 PACS number(s): 47.54.−r, 47.51.+a, 47.65.Cb, 68.15.+e

I. INTRODUCTION

Complex pattern formation abounds in nature and has been actively studied in many different physical, chemical, and biological systems [1–3]. One major point of interest is to try to understand the morphology of the rising patterns and look for possible universalities. In this context, the investigation of growth phenomena in ferrofluids has drawn considerable attention [4,5]. A ferrofluid is a colloidal suspension of nanometer-sized magnetic particles in a suitable nonmagnetic carrier liquid. Due to its unique response to applied magnetic fields, this fluid material has become a prototypical dipolar system for the study of a number of pattern-forming processes and interfacial instabilities [6,7].

The behavior of a ferrofluid surface is critically dependent on the direction and magnitude of the applied magnetic field. When the initially flat free surface of a ferrofluid film is subjected to a uniform perpendicular magnetic field, the Rosensweig instability [8] takes place and a hexagonal array of peaks arises. A perpendicular magnetic field is also responsible for the formation of intricate labyrinthine structures if a ferrofluid sample is confined between closely spaced parallel plates of a Hele-Shaw cell [9]. In a laboratory this perpendicular field configuration can be readily generated by a pair of identical Helmholtz coils whose electric currents have the same magnitude and flow in the same direction.

Due to its relatively easy practical implementation the perpendicular field arrangement has been largely utilized to investigate both experimentally and theoretically various aspects of the classic Rosensweig and labyrinthine instabilities. These studies revealed a broad range of phenomena ranging from the formation of solitonlike structures [10] or wave turbulence [11] on the surface of the magnetic fluid, and the breakup of peaks into separate droplets in very thin ferrofluid films [12], through the simultaneous appearance of labyrinths and peaks if the ferrofluid is miscible with its surroundings [13].

Nevertheless, the potential of the Helmholtz coils setup in providing nice pattern-forming structures in magnetic fluids has not been exhausted. Very recently a theoretical study [14] has proposed that simply by reversing the direction of the current in one of the coils ("anti-Helmholtz" arrangement [15]), one could produce a very simple but innovative magnetic-field disposition. Under such circumstances, a purely radial magnetic field would act in the midplane between the coils. In this work we implement the experimental arrangement related to this radial field setup and perform a series of experiments that consider the action of the field on the time evolution of a thin, miscible ferrofluid droplet. This particular experimental layout has the great advantage of allowing, with the same experimental setup commonly used to produce the traditional perpendicular field, the generation of interfacial patterns presenting very different and appealing morphologies. As a result, still unexplored growth processes and possible universal behaviors can be unveiled and discussed.

II. EXPERIMENTAL RESULTS AND DISCUSSION

A. Radial magnetic field: Experimental setup

Our experimental setup is sketched in Fig. 1. An initially circular, millimeter-sized ferrofluid droplet is placed at the center of a cylindrical, horizontal cavity, whose diameter and

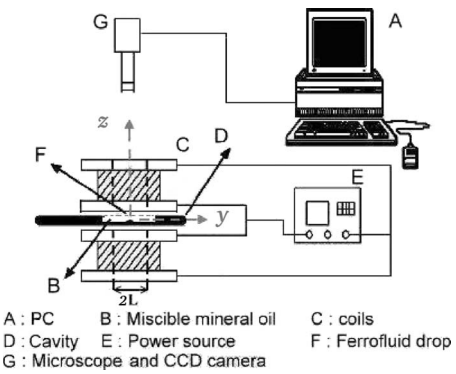

FIG. 1. Scheme of the experimental setup.

*chingyao@mail.nctu.edu.tw
†jme@df.ufpe.br

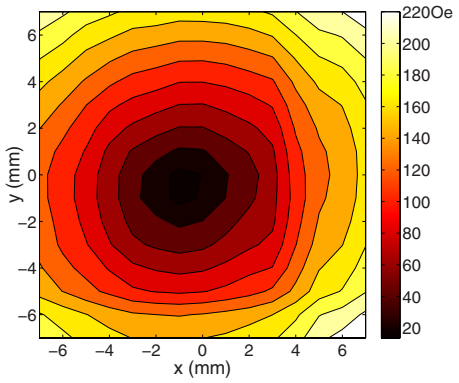

FIG. 2. (Color online) Distribution of magnetic-field strength on the x-y plane (plane of the cavity) for $I=2.6$ A.

depth are 2 cm and 1 mm, respectively. A coordinate system (x,y,z) is defined in such a way that its origin is located at the center of the cavity which lies on the x-y plane. Due to the dominance of surface tension at such a small scale, the ferrofluid droplet has the shape of a spherical cap with a typical contact angle of about $18\pm2°$. The characteristic maximum height of the spherical cap is on the order of 0.3 mm. The cavity is then slowly filled with a nonmagnetic miscible fluid, so that the ferrofluid droplet is completely immersed in a thin layer of such a solvent. Once the cavity is filled with the miscible solvent, the ferrofluid droplet no longer forms a spherical cap but acquires a flatter profile and a more elongated shape. The typical time between the filling with the miscible solvent and the beginning of the experiments (when the external magnetic field is turned on) is about 5 s.

The magnetic fluid we use is a light mineral oil-based commercially available ferrofluid (EMG901) produced by Ferrotec. The viscosity and density of the ferrofluid are $\eta_d=10$ cp and $\rho_d=1.53$ g/ml, respectively. The surrounding nonmagnetic liquid is a particular type of mineral oil (carrier fluid of the ferrofluid EMG911) with $\eta_m=4$ cp and $\rho_m=0.89$ g/ml. A radial magnetic field H_r is generated by a pair of coils (coaxial with the z axis) in an anti-Helmholtz configuration. Because of the coil's body, the observing range is limited by the central hole of the coils whose radius is $L=7.5$ mm.

Shown in Fig. 2 is a typical magnetic-field distribution in the x-y plane, measured by a SYPRIS 6010 Gaussmeter with a 1 mm$\times$1 mm resolution, for an electric current $I=2.6$ A in the coils. The three components of the magnetic field H_x, H_y, and H_z are measured and the intensity of the radial magnetic field $H_r=[H_x^2+H_y^2]^{1/2}$ is calculated. We have observed that $H_z\approx8$ Oe at the edges of the coils and $H_z\approx4$ Oe at the coils center. On the other hand, the average radial magnetic-field strength at the coils is $H_r=147$ Oe, thus $H_r\gg H_z$, and the influence of H_z can be safely neglected.

One of the most challenging aspects of our experiment refers to the search for an exactly axisymmetric radial magnetic field distribution on the plane of the cavity. The almost unavoidable misalignment of the cavity with respect to the actual x-y plane is an important practical impediment. Another limitation is the imperfect manufacturing of the coils. Despite these difficulties, the magnetic-field distribution depicted in Fig. 2 grows almost linearly with the radial distance r and can be approximated as

$$\mathbf{H}\approx H_r\hat{\mathbf{r}}=\frac{H_0}{L}r\hat{\mathbf{r}}, \tag{1}$$

where $\hat{\mathbf{r}}$ is a unit vector in the outward radial direction and H_0 represents the average field strength at $r=L$. We consider three different field strengths $H_0=102$, 124, and 147 Oe which correspond to the currents $I=1.8$, 2.2, and 2.6 A, respectively.

From a theoretical point of view, the structure of the magnetic field in the x-y plane as expressed by Eq. (1) follows from $\nabla\cdot\mathbf{H}=0$ and the homogeneity of the z component of the magnetic field, so that the total magnetic field could be written as $\mathbf{H}(r,z)=H_r(r)\hat{\mathbf{r}}+H_z(z)\hat{\mathbf{z}}$. Moreover, for the anti-Helmholtz arrangement, a simple calculation for the magnetic field between the coils to lowest order in both r and z, and considering that $z\ll r$ results in a convenient relation

$$\frac{H_r}{H_z}\sim-\frac{1}{2}\frac{r}{z}, \tag{2}$$

where the negative sign is related to the fact that H_z changes direction when one crosses the x-y plane. The theoretical prediction we obtained in Eq. (2) is in very good agreement with our experimental measurements for the magnitudes of the magnetic-field components H_r and H_z, in which $H_r\gg H_z$.

The time evolution of the diffusing interface separating the two miscible fluids is directly recorded from above by a charge coupled device camera, providing an upper view of the situation. The camera is connected to a microscope so that the pictures can be properly enlarged and recorded, and then transmitted to a computer for further analysis. Notice that whenever we talk about a miscible "interface" we really mean the mixing region between the miscible fluids. In the regions of significant concentration gradients, the concept of an interface is still meaningful and well represented [13].

B. Pattern evolution

Even though we have performed a large number of experiments (35 in total) using various initial droplet diameters and three distinct magnetic field strengths H_0, for the sake of clarity we illustrate our results focusing on a reduced set of experiments. This is done without loss of generality since the results we present are quite robust and consistent with the totality of our measurements.

Figure 3 illustrates the interfacial evolution of a ferrofluid droplet under the field condition $H_0=147$ Oe. The original diameter of the droplet before mixing with the solvent is about 3.81 mm. It should be noted that before adding the solvent, the ferrofluid droplet remains circular even at the maximum field strength available. For our system, interfacial instabilities only appear in the presence of mixing. Here we address another experimental difficulty, namely, the one involved with the estimation of the droplet initial diameter. Since mixing occurs immediately upon the contact of the fluids, there always exist inaccuracies regarding how to con-

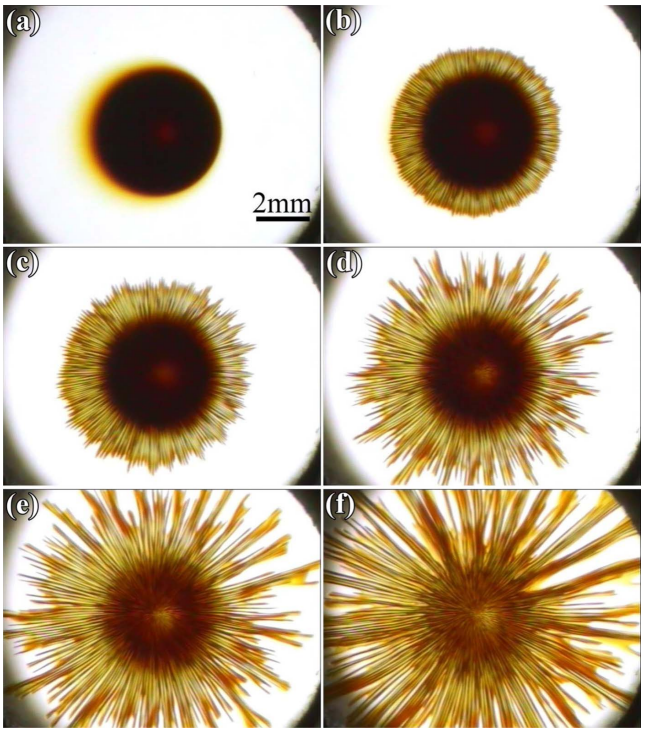

FIG. 3. (Color online) Snapshots of top views for $d=5.12$ mm and $H_0=147$ Oe at (a) $t=0$, (b) $t=0.4$ s, (c) $t=0.8$ s, (d) $t=1.2$ s, (e) $t=1.6$ s, and (f) $t=2.4$ s.

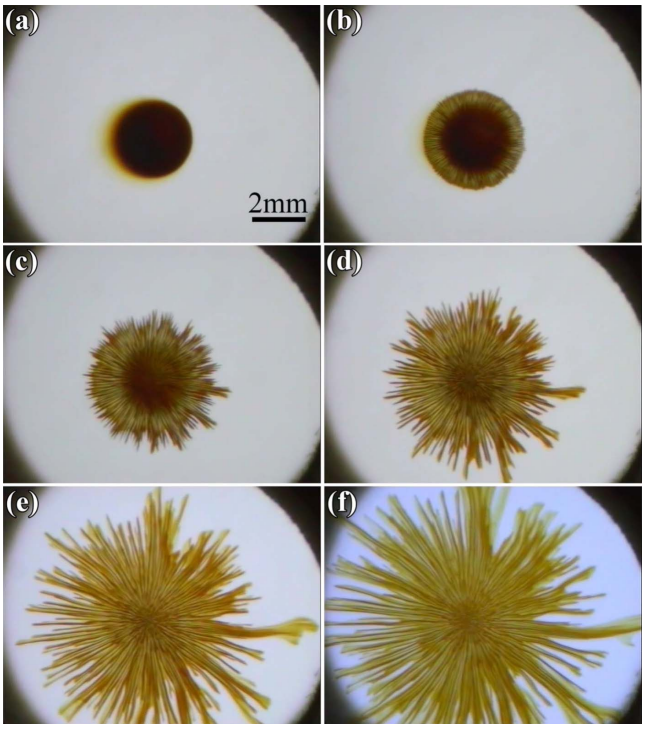

FIG. 4. (Color online) Snapshots of top views for $d=3.27$ mm and $H_0=147$ Oe at (a) $t=0$, (b) $t=0.8$ s, (c) $t=1.6$ s, (d) $t=2.4$ s, (e) $t=4.0$ s, and (f) $t=5.6$ s.

trol and measure the initial condition of the problem.

In order to properly take into account the important initial mixing effects, the image immediately before the field is applied [$t=0$ s in Fig. 3(a)] is scanned into a MATLAB image treatment software of 640×480 pixels whose resolution is of 18 μm. The mixing area occupied by the ferrofluid can then be represented by the correspondent low grayscale intensity values, and the entire initial droplet area can be more precisely estimated, once a representative grayscale intensity threshold is established. A more detailed discussion about the evaluation of the droplet area will be presented in Sec. II C. As a result of this procedure, a correspondent initial effective diameter of $d=5.12$ mm is obtained. This effective diameter is significantly larger than the diameter measured before mixing (approximately a 40% increase in diameter) demonstrating the importance of mixing effects right from the beginning of the process.

The reasons for this increase in diameter might be attributed to three different factors, namely, diffusion, convective transport, and reduction in contact angle. In principle, diffusion would lead to instantaneous mixing once the ferrofluid makes contact with the miscible solvent and thus would enlarge the area occupied by the ferrofluid droplet. The increment in diameter due to diffusion can be roughly estimated as follows. If we consider an one-dimensional diffusion problem whose initial condition for the concentration is $c(x,0)=1$ for $|x|<1$, and $c=0$ elsewhere, associated with the boundary conditions $c(x,t)=0$ at $x=\pm\infty$, the analytical solution for the time-dependent concentration field can be expressed in terms of an error function [16]

$$c(x,t)=\frac{1}{2}\left\{\mathrm{erf}\left[\frac{(1-x)}{2\sqrt{kt}}\right]+\mathrm{erf}\left[\frac{(1+x)}{2\sqrt{kt}}\right]\right\}, \tag{3}$$

where k denotes the diffusion constant. If we use a typical value for the diffusion coefficient [17,18] $k=10^{-10}$ m^2/s, take the concentration front $c=0.01$, and consider the characteristic time $t=5$ s (typical time between the filling of the cavity with the miscible solvent, and the beginning of the experiments at nonzero field), Eq. (3) gives us an increment in diameter of about 0.15 mm (or less than 4%) for the droplet considered in Fig. 3. Note that if we take a higher value of concentration, the result would be an even smaller increase in the droplet's diameter. On the other hand, longer times would lead to higher diffusive advancement of the concentration front. However, the bottom line is that in our experiments, the initial increase in diameter exclusively due to diffusive effects is indeed very small.

A second contributing factor for the increase in diameter is the convective transport associated with the unavoidable flow induced by the filling process. This convective effect can be detected by inspecting the blurred region located on the left side of the droplets at $t=0$ [see Figs. 3(a) and 4(a)]. This is due to the orientation of filling process, which begins on the left-hand side of the cavity. However, we tried to minimize this effect as much as possible by performing the filling of the cavity in a very slow rate. So, this effect is not expected to be that significant either. Therefore, we believe that the major factor causing the sizable change in the initial droplet diameter is most probably due to the abrupt decrease in surface tension associated to a progressive reduction in

contact angle during the filling process. Unfortunately, a more quantitative estimate of this last effect is very difficult to be obtained under the circumstances of our experiments, in which the droplet profile shape, the contact angle, and the surface tensions involved are extremely hard to be evaluated during the initial mixing process and thereafter.

Returning to Fig. 3, we notice that immediately after the magnetic field is turned on, very active fingering patterns emerge at the rim of the droplet [Fig. 3(b)]. The outer circumferential region of the droplet spreads outward leading to the formation of numerous extremely fine fingers. At this stage, the dark central region of the droplet is not significantly affected and retains its original nearly circular shape. We point out that later in the text, a more precise and quantitative definition will be given to the grayscale intensity in our problem that will be defined as being minimum for the darkest spot in the ferrofluid and maximum at the nearly transparent background region.

The formation of fingers observed in Figs. 3 and 4 can be associated to the occurrence of a number of important processes: the existence of a local magnetic force, the role played by viscous forces, and three-dimensional (3D) thinning effects. On top of these, diffusive effects also play a role. The radial magnetic force density is expressed as [4,19,20]

$$f_m = \mu_0 c M \nabla H_r, \tag{4}$$

where μ_0 is the free space permeability, c is the local concentration of the ferrofluid, and M denotes the ferrofluid magnetization. The area expansion experienced by the viscous ferrofluid is accompanied the simultaneous thinning of the ferrofluid film thickness in the vertical direction. Since the more viscous fluid (ferrofluid) displaces the less viscous one (solvent), the outward pattern motion tends to be stabilized by viscous effects. Diffusion naturally leads to variation in local concentration, which in turn influences the local magnetic force and the viscosity, since both depend on the concentration. It is common to evaluate the influence of diffusion by considering the dimensionless Péclet number $\mathrm{Pe} = Ud/k$, where U is the average expanding velocity of the mixing boundary, d is the initial droplet diameter, and k is a diffusion constant. By using typical values associated to our experiments, where $d \sim O(\mathrm{mm})$, $k \sim O(10^{-10}\ \mathrm{m}^2/\mathrm{s})$, and $U \sim O(\mathrm{mm/s})$ we obtain that $\mathrm{Pe} \sim O(10^4)$.

The Péclet number is used to evaluate the relative importance of mass and concentration transport effects. It is defined as the convective velocity over the diffusive velocity. The fact that we have found a Péclet number on the order of 10^4 indicates that the transport of the ferrofluid by convection is considerably stronger than the one induced by diffusion. However, since we are dealing with a miscible interface which involves a magnetic fluid, the connection between diffusive and magnetic effects will make diffusion to have a relevant role in the pattern formation process. The emergence of an enormous number of tiny (peaky) fingering structures already at very early time stages of pattern formation [Figs. 3(b) and 4(b)] is a consequence of the action of magnetic forces under nearly zero surface tension conditions. Once this scenario of multiple peaked structures is established it "leaves its mark," in the sense that the whole subsequent time evolution of the pattern morphology will be influenced by this initial interaction between diffusive and magnetic contributions. If surface tension was nonzero (immiscible ferrofluid flow), one should expect a considerably smaller number of emerging fingers presenting tips that should have been notably less sharp. This is exactly the kind of starfish-like patterns theoretically obtained when an immiscible ferrofluid droplet is subject to a radial magnetic field in the confined environment of a Hele-Shaw cell (see Ref. [14]). In this sense, although we are dealing with such a high magnitude for the Péclet number, diffusion also plays an important role in setting the pattern morphology under the miscible ferrofluid circumstances we study in this work.

The local magnetization in a ferrofluid can be well approximated by a linear relation $M(r) = \chi H_r(r)$, where χ represents the magnetic susceptibility. By using this relation plus Eqs. (1) and (4) one obtains that

$$f_m(r) = \mu_0 c \chi \left(\frac{H_0}{L}\right)^2 r. \tag{5}$$

Therefore, the outer circumferential region of the droplet in Fig. 3(b) is subjected to a maximum outward force, while its central region is not as affected. It is interesting to note that this magnetically induced mechanism is similar to the centrifugally driven effects occurring in immiscible rotating fluid flows [21] and spin coating processes [22]. However, our system is more complex since it involves the simultaneous interplay of magnetic, viscous, and diffusive effects under nearly zero surface tension circumstances.

Although the precise determination and measurement of the ferrofluid film thickness along the z axis is not an easy task, qualitative observations of the droplet profile indicate that its thickness varies with the radial distance: it is maximum at the center of the droplet and decreases as one approaches the border of the droplet. These 3D features affect the evolution and the ultimate shape of patterns observed in Figs. 3 and 4. Further discussion about these 3D effects will be addressed in Sec. II C. The existence of stronger magnetic forces at lower thickness regions of the droplet leads to significant local fluid stretching. While very active fingering phenomena are triggered by the stronger magnetic forces, more dilute ferrofluid concentration results from the stretching of the lower thickness regions. As a result, numerous fine fingers are formed within a lighter annular region at this early stage of pattern formation [Fig. 3(b)].

As time evolves to $t=0.8$ s [Fig. 3(c)] the spreading process proceeds and the lighter mixing region keeps expanding. Affected by local magnetic forces, and by the continuous stretching of the mixing boundary, the ferrofluid located at the central region of the droplet starts to move outward. This is indicated by the shrinkage of the dark circular ferrofluid region. The outward motion of the inner parts of the droplet supplies a sufficient amount of ferrofluid to expand, so that the pattern keeps its overall circular shape. However, as time proceeds to $t=1.2$ s [Fig. 3(d)] the outward stretching is much more vigorous due to stronger magnetic forces. While the dilute mixing fringe keeps expanding, and the core region shrinks further, fingers merge and compete. As finger

merging is favored by diffusion, increased competition is maintained by radially growing magnetic effects. As a result of these processes, the circular shape cannot be sustained and visually striking starburstlike patterns arise [Figs. 3(d) and 3(e)]. It is worth pointing out that the relatively sudden transition from a nearly circular envelope [Fig. 3(c)] to a quite uneven boundary [Fig. 3(d)] has a parallel with phenomena occurring in immiscible spin coating processes [22–25]. In the latter, there exists a critical radius, beyond which irregular interfacial fingering emerges and finger competition takes over. Regarding the peculiar morphology of the resulting patterns, we note that similar starlike shapes have been theoretically predicted to arise in immiscible ferrofluids under a radial magnetic field in Ref. [14]. However, for the miscible situation depicted in Figs. 3(d) and 3(e) the spikes can become very long and thin, since the surface tension is practically zero. Starfishlike structures have also been observed in experiments considering the action of fast rotating magnetic fields on immiscible ferrofluid droplets [26,27].

There is in fact a more direct connection between the centrifugal force in rotating fluid systems and the magnetic force produced by a radial magnetic field. For example, notice that both forces point outward and increase linearly with the radial distance r. This has been originally discussed in Ref. [14] where exact solutions for the shape of immiscible, rotating Hele-Shaw cell patterns are obtained as a low magnetic susceptibility limit of the corresponding patterned structures obtained in immiscible ferrofluids subjected to a radial magnetic field. However, a more quantitative parallel between our current miscible experiments and the ones in spin coating systems is still unavailable. The existing spin coating experiments (Refs. [22–25]) have been performed by using immiscible liquids, so the patterns found are not exactly similar to the ones we have obtained in our miscible ferrofluid experiments under radial field conditions. A comparison of our miscible patterns with those obtained by numerical simulations of miscible fluids in rotating Hele-Shaw cells [21] also shows fundamental differences. This is not surprising since in Hele-Shaw cells the confined flow takes place at constant thickness (absence of thinning effects) and conserves the droplet area. Nevertheless, the connection between our current radial field experiments and the ones in spin coating system is certainly a very interesting issue that deserves further attention from both experimentalists and theorists.

Continuing the analysis of Fig. 3, we observe that once a particular set of outward "winning" fingers are formed, the motion of the remaining ferrofluid material totally follows their routes. At this point [Fig. 3(f)], finger merging keeps acting and a reduced number of slimmer fingers evolve consistently throughout late growth stages. We point out that the pattern evolution represented in Fig. 3 is quite robust and valid for droplets whose diameters are larger ($d>4$ mm). Regardless various conditions of the applied field strengths and initial diameters, the overall fingering patterns of these larger droplets show great qualitative similarities.

A representative case for the time evolution of smaller droplets ($d<4$ mm) is shown in Fig. 4 for $d=3.27$ mm and $H_0=147$ Oe. Due to the smaller radial dimension of the droplet, the local magnetic force is weaker. Consequently, the outward motion of the pattern is significantly slower compared to the larger droplet situation shown in Fig. 3. As in Fig. 3, the pattern morphologies shown in Fig. 4 change from circular at zero field to starburstlike structures at finite field. However, one easily identifiable difference is the fact that after $t=2.4$ s [Fig. 4(d)], the central ferrofluid core nearly disappears and all the mixing region shows a quite uniform concentration distribution. This can be verified by the similar brightness in the entire image of the patterns depicted in Figs. 3(e) and 3(f). Once there is no significant fluid accumulation in the core to provide a uniform outward expansion of the droplet, a more intense finger competition is triggered. Notice that although the finger competition process in smaller droplets is delayed in comparison to what happens to larger droplets, it eventually takes place. The decrease in ferrofluid accumulation at the core region suggests that the expansion of smaller droplets is closely related to the progressive thinning of the ferrofluid film thickness. Therefore, a more evenly distributed spreading of the inner portions of the pattern is observed. This distinction can be clearly verified by contrasting Figs. 3(f) and 4(f): while parts of the nonmagnetic fluid occupy the inner droplet body in Fig. 3(f), the central region of the pattern shown in Fig. 4(f) is fully occupied by a more dilute ferrofluid. So, by comparing Figs. 3 and 4 we can find both differences at earlier stages (delayed finger competition) and similarities (formation of starlike structures) for longer times. Once again, we stress that the pattern evolution depicted in Fig. 4 is quite similar to all other experiments we have performed for smaller droplets.

C. Growth and scaling

The quantitative analysis of the complex miscible fingering process studied in this work is not a trivial task. Unlike similar immiscible growth processes, in which nonzero surface tension leads to a sharp and well-defined fluid-fluid interface, here the fingering structures can be much thinner and diffuse due to mixing. Nevertheless, in the region of significant concentration gradient, the concept of an interface can still be well represented. This is in part provided by the significant visual contrast between the ferrofluid (very dark liquid) and the solvent (clear fluid), even at the outermost mixing region. In this sense, one can try to measure the pattern growth by examining the time evolution of the area occupied by the mixture containing the ferrofluid. A similar type of approach is frequently utilized to describe the time evolution of the typical size of fluid patterns in immiscible spin coating processes [22–25]. Likewise, here we take the area of the evolving droplet is a suitable measure of its growth.

As commented at the beginning of Sec. II B we can determine the area of the evolving pattern by applying a threshold intensity to a grayscale image of the growing droplet and counting all those image pixels with intensities falling below this threshold. With this concept in mind, we use a MATLAB image treatment software and graduate the intensity of grayscale, denoted as I_g, between 0 (the darkest spot) and 1 (the background region), so that $0 \leq I_g \leq 1$. The particular grayscale intensity distributions along the y axis for the times and

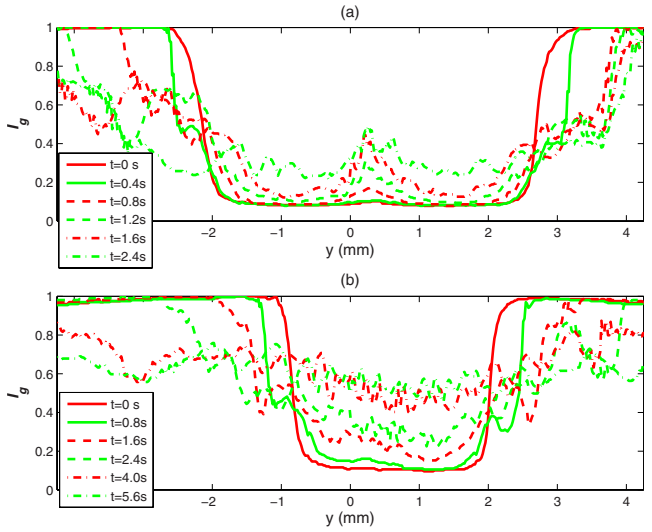

FIG. 5. (Color online) Distribution of the grayscale intensity I_g along the y axis for the experimental situations shown in (a) Fig. 3 and (b) Fig. 4.

patterns presented in Figs. 3 and 4 are depicted in Figs. 5(a) and 5(b), respectively. In Fig. 5(a), the initial intensity distribution at $t=0$ shows a clear flat valley in the central region (ferrofluid droplet body) presenting a steep increase to the background intensity at $I_g=1$. Due to the mixing nature of the flow, the transition from lower to higher values of I_g becomes less and less abrupt as time progresses. A similar scenario is observed for smaller droplets as illustrated by Fig. 5(b). These findings can be related to the 3D thinning effects which take place at the evolving ferrofluid droplet as mentioned in Sec. II B. The variation in grayscale intensity indicates a change in the thickness of the droplet as time advances. Note that for a smaller droplet [Fig. 5(b)] the transition in I_g is typically smoother than the one observed for a larger ferrofluid droplet [Fig. 5(a)]. This reinforces the idea of a more uniform 3D thinning effect occurring in smaller droplets as pointed out in Sec. II B. It is worth noting that the peaks appearing in the central region of Fig. 5(a) are mainly due to the light source located on top and at the center of the cavity, as can also be seen by inspecting Fig. 3.

From the discussion of Fig. 5 it is evident that the grayscale intensity offers a viable method to evaluate the area of the mixing ferrofluid patterns once a particular threshold value for I_g is determined. To have a more quantitative assessment of the pattern growth process, in Fig. 6 we analyze how the area occupied by the ferrofluid varies with time, by taking a characteristic threshold value $I_g=0.80$. The justification for this particular choice for the threshold will be discussed at the end of this section. Two typical sets of droplet sizes with effective diameters around 5 and 3 mm are presented. The evolution of the actual areas is displayed in Fig. 6(a). As one would expect, faster growth occurs for larger droplets or stronger field strengths. If time is rescaled by $\tau = \eta_d L^2/\mu_0 d^2 H_0^2$, and area by the initial droplet area $A_0 = \pi d^2/4$, the dimensionless evolution of the rescaled area $A' = A/A_0$ and time $t' = t/\tau$ is depicted in Fig. 6(b). Two distinct groups of collapsing curves are observed, one for smaller droplets and a second for larger ones. This is consistent with the qualitative observations presented in the discussion of Figs. 3 and 4 and also by the more quantitative account shown in Fig. 5. The more significant growth for smaller droplets observed in Fig. 6(b) is related to their more uniform growth induced by 3D film thinning, which results in an increased area covered by the ferrofluid.

However, a more interesting behavior can be found if we consider the time evolution of the area increment $\Delta A = A - A_0$ defined as the difference between the time-dependent area A and its value at $t=0$. Figure 6(c) plots the dimensionless area increment $\Delta A' = A' - 1$ as a function of t'. We can see that the memory of initial conditions is lost for larger times ($t' > 5000$) and that the evolution of $\Delta A'$ is universal defining a regime where both larger and smaller droplets follow a common power-law behavior $\Delta A' \sim t'^{4/3}$. The reason for the convergence of both smaller and larger droplets to a common power-law growth at longer times can be related to the mechanism of finger competition: it occurs quite sooner for larger droplets, so that a universal growth is reached at earlier times. On the other hand, a smaller droplet remains nearly circular and without strong signs of finger competition at earlier times appearing to follow a different growth behavior. Nevertheless, the growth of smaller drop-

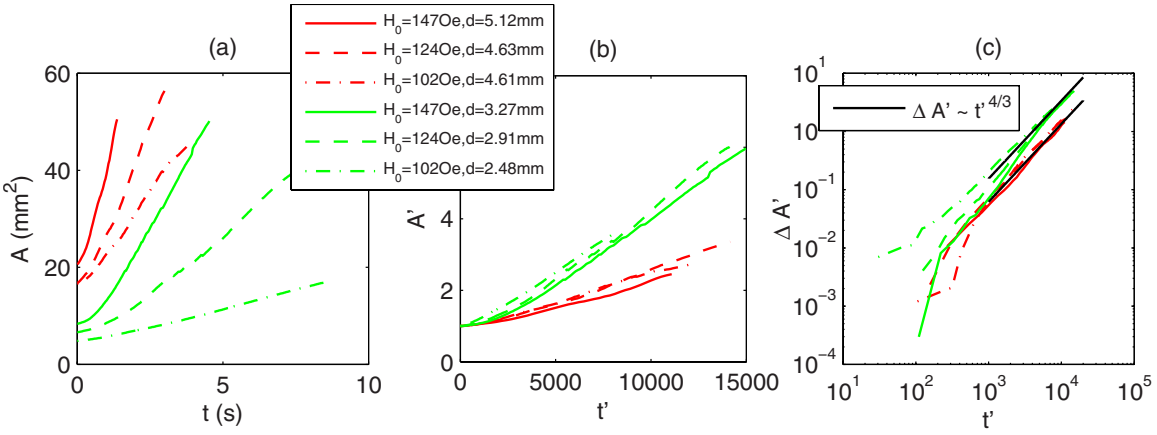

FIG. 6. (Color online) Time evolution of expanding area in (a) dimensional form and (b) dimensionless form. The evolution of the area increment $\Delta A' = A' - 1$ is shown in (c).

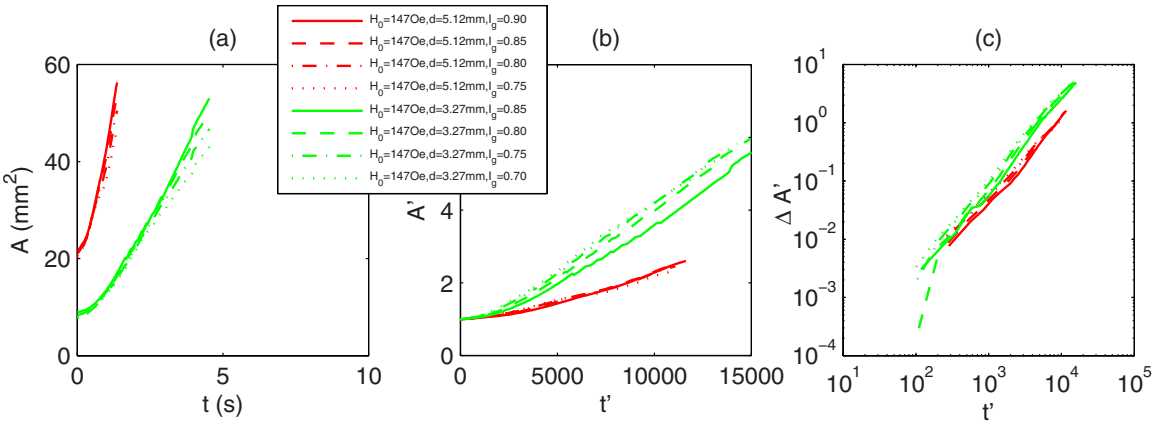

FIG. 7. (Color online) Time evolution of (a) A, (b) A', and (c) $\Delta A'$ for various grayscale intensity thresholds I_g. The magnetic-field magnitude and the droplet's diameters are related to the experiments presented in Figs. 3 and 4.

lets will eventually follow a 4/3 power law at longer times, when finger competition events are favored.

The so-called "finger competition" events mentioned above deserve further clarification: they are related to the nonuniform growth of the fingers, in which the diffusive interface does not expand in an overall circular fashion. It should be noticed that the miscible interface will remain fairly circular (despite the existence of multiple tiny peaks) if the mass addition from the thinning effects is sufficient to cover the expanding area in the plane of the flow. Only when the expanding rate is too high, and the mass supply is no longer enough to maintain a circular expansion, will the finger competition events take place. Since the expanding rate, which depends on the local magnetic force and increases with time when the radial distance grows, the finger competition phenomena would eventually happen for droplets of all sizes, being just a matter of time or location. A similar notion is also defined for immiscible systems (e.g., in spin coating experiments [25]), where a maximum distance to have the rising and competition among the fingers is an important factor called "critical diameter." For a bigger droplet, the expanding rate is much larger due to its initial larger distance from the origin. In addition, the thinning effect is not that significant as shown in Fig. 5. Very soon, the additional volume of fluids is no longer sufficient to maintain the needs of a uniform circular expansion of the droplet. As a result, only a limited number of dominant fingers can keep growing, while the growth of the remaining fingers is inhibited. This characterizes a finger competition event. On the other hand, for a smaller droplet, due to its initially shorter radial distance from the field origin, and more significant thinning effects, the stable circular expansion lasts for a longer time period. However, finger competition would happen once the interface has grown far away from the origin. We believe this can be a possible reason why the growth rate for the smaller droplets at earlier time is greater than the one of larger droplets. Nevertheless, in a long run a similar finger competition scenario occurs both for larger and smaller droplets. In this sense, this finger competition mechanism may serve as a qualitative (but not at all final) explanation for the similar growth scaling of droplets of different sizes at late times.

Despite the fact that Fig. 6 just presents six different parameter sets, we stress that we have actually performed a much larger number of systematic experimental runs and all of them reproduce quite well the main features illustrated in Fig. 6. Most importantly, the power-law behavior $\Delta A' \sim t'^{4/3}$ is consistently found in all experiments we have performed. By extracting data from the 35 experiments we performed for different initial droplet diameters we obtained pretty much the same behavior, in which the mean value for the power-law exponent was 1.3354, with standard deviation equal to 0.0638. In this sense, the behavior depicted in Fig. 6 is representative of an extensive set of experimental data.

The power-law behavior obtained in Fig. 6(c) stands between the limits of normal diffusion ($\sim t$) and ballistic motion ($\sim t^2$) [28]. A slower growth behavior ($\sim t^{2/3}$) has also been estimated for immiscible spinning droplets [22]. The smaller growth for this immiscible rotating flow is justified by the presence of a nonzero surface tension. All this seems quite reasonable since in our miscible system we have a sort of magnetically assisted diffusion process.

We conclude this section by examining the behavior of the quantities A, A', and $\Delta A'$ if one assumes different values of the grayscale intensity threshold. This will also allow us to test the robustness of the power-law growth detected in Fig. 6(c). The smooth transitions in I_g illustrated in Fig. 5 indicate that the determination of the actual area of the evolving pattern from the grayscale intensity could not be uniquely determined. After all, since the droplet boundary is not sharp, it is reasonable to expect that the apparent size of the droplet would depend on the particular threshold intensity used. In order to verify this very important point, in Fig. 7 we plot how A, A', and $\Delta A'$ vary with time, considering the physical parameters related to the growth of the patterns presented in Figs. 3 and 4. This is done by taking different values of the grayscale intensity threshold I_g. It is evident that the exact numerical values of A, A', and $\Delta A'$ are slightly altered as the intensity threshold is changed. For example, in Fig. 7(a) we can see that larger droplet areas result if higher threshold values are used. However, it is also clear that the overall trends are all quite consistent, so that the general description for the behavior of the droplet does not depend strongly on the choice of the threshold. Most importantly, as illustrated in Fig. 7(c), despite the changes in the threshold, we have verified that the scaling behavior $\Delta A' \sim t'^{4/3}$ as exemplified in Fig. 5(c) still holds. Once again, we emphasize that all

these conclusions have been tested for a larger set of experiments, which are all consistent with the illustrative cases considered in Fig. 7. This important verification substantiates the robustness of the scaling we have found pointing to the appropriateness of our quantitative approach based on the grayscale intensities.

III. CONCLUSION

In this work we have described the behavior of a thin ferrofluid droplet surrounded by a miscible nonmagnetic fluid. When the system is placed in the midplane between the two coils of an anti-Helmholtz apparatus, the droplet experiences a purely radial magnetic field and therefore spreads forming starlike patterns. Our experimental data are analyzed based on a number of measurements which consider various different initial droplet diameters and three typical magnetic strengths.

The pattern formation system can be reasonably (but not yet quantitatively) understood by considering the interplay of magnetic, diffusive, convective, and viscous effects. The magnetic effects work to activate the rising of the tiny initial peaks at the diffusing interface similarly to what happens in the classical Rosensweig instability in ferrofluids [4,5,8]. Diffusion leads to changes in the local concentration, and consequently both the local viscosity and magnetization (or, alternatively the magnetic force) are also modified since these quantities are all concentration dependent. On top of these effects, the variations in viscosity and magnetic force lead to a locally varying convective motion of the fluids, leading to the rising of numerous long thin spikes. Within this complicated scenario a universal 4/3 power-law behavior is found for the long time evolution of the droplets' area increments.

All the physical effects mentioned above certainly interact with each other, however, in a very complex way which cannot be easily singled out. Unfortunately, at this point in our research we are not able to access the details of the coupling among these various effects. A more detailed quantitative description of the complicated growth process revealed by our experiments requires a better knowledge of the pattern's time evolution. Although a theoretical treatment of the influence of long-range magnetic forces on diffusive processes is challenging, we hope our work will stimulate further research on this topic.

During the course of this work, we learned about an unexpected morphological similarity between our miscible ferrofluid patterns under radial magnetic fields, and magnetohydrodynamic structures formed on the surface of the Sun, known as sunspots [29]. Sunspots are dark plasma regions on the solar surface that are often accompanied by bursts of activity resulting in the emergence of interesting filamentary structures directed along the radial direction. A relatively recent theoretical model [30] suggests that the pattern structures appearing in sunspots are the result of the local interaction between an intense radial magnetic field and complex convective processes. Despite the obvious phenomenological differences between our system and the one related to sunspots, the fact that similar patterns are obtained and that both problems involve magnetohydrodynamics under radial magnetic fields raises the question of a deeper connection. As in Ref. [31] ferrofluids might be useful in providing a possible terrestrial laboratory for the study of sunspot pattern formation.

ACKNOWLEDGMENTS

J.A.M. thanks CNPq (Brazilian Research Council) for financial support of this research through the program "Instituto Nacional de Ciência e Tecnologia de Fluidos Complexos (INCT-FCx)" and also through the CNPq/FAPESQ Pronex program. C.-Y.C. thanks the National Science Council of the Republic of China for financial support through Grant No. NSC 96-2221-E-009-244-MY3.

[1] P. Pelcé, *Dynamics of Curved Fronts* (Academic, Boston, 1988).
[2] H. Meinhardt, *Models of Biological Pattern Formation* (Academic, New York, 1982).
[3] M. C. Cross and P. C. Hohenberg, Rev. Mod. Phys. **65**, 851 (1993).
[4] R. E. Rosensweig, *Ferrohydrodynamics* (Cambridge University Press, Cambridge, 1985).
[5] E. Blums, A. Cebers, and M. M. Maiorov, *Magnetic Fluids* (de Gruyter, New York, 1997).
[6] M. Seul and D. Andelman, Science **267**, 476 (1995).
[7] C. Rinaldi, A. Chaves, S. Elborai, X. He, and M. Zahn, Curr. Opin. Colloid Interface Sci. **10**, 141 (2005).
[8] M. D. Cowley and R. E. Rosensweig, J. Fluid Mech. **30**, 671 (1967).
[9] A. J. Dickstein, S. Erramilli, R. E. Goldstein, D. P. Jackson, and S. A. Langer, Science **261**, 1012 (1993).
[10] R. Richter and I. V. Barashenkov, Phys. Rev. Lett. **94**, 184503 (2005).
[11] F. Boyer and E. Falcon, Phys. Rev. Lett. **101**, 244502 (2008).
[12] C.-Y. Chen and Z. Y. Cheng, Phys. Fluids **20**, 054105 (2008).
[13] C.-Y. Chen, W. K. Tsai, and J. A. Miranda, Phys. Rev. E **77**, 056306 (2008).
[14] R. M. Oliveira, J. A. Miranda, and E. S. G. Leandro, Phys. Rev. E **77**, 016304 (2008).
[15] T. H. Bergeman, G. Erez, and H. J. Metcalf, Phys. Rev. A **35**, 1535 (1987).
[16] E. Kreyszig, *Advanced Engineering Mathematics* (Wiley, New York, 1998).
[17] P. Petitjeans and T. Maxworthy, J. Fluid Mech. **326**, 37 (1996).
[18] J. B. Segur, in *Glycerol*, edited by C. S. Miner and N. N. Dalton, (Reinhold, New York, 1953).
[19] M. Igonin and A. Cebers, Phys. Fluids **15**, 1734 (2003).
[20] C.-Y. Chen and H.-J. Wu, Phys. Fluids **17**, 042101 (2005).
[21] C.-Y. Chen, C.-H. Chen, and J. A. Miranda, Phys. Rev. E **73**,

046306 (2006).
[22] F. Melo, J. F. Joanny, and S. Fauve, Phys. Rev. Lett. **63**, 1958 (1989).
[23] N. Fraysse and G. M. Homsy, Phys. Fluids **6**, 1491 (1994).
[24] M. A. Spaid and G. M. Homsy, Phys. Fluids **9**, 823 (1997).
[25] M.-W. Wang and F.-C. Chou, J. Electrochem. Soc. **148**, G283 (2001).
[26] J.-C. Bacri, A. Cebers, and R. Perzynski, Phys. Rev. Lett. **72**, 2705 (1994).
[27] A. V. Lebedev, A. Engel, K. I. Molozov, and H. Bauke, New J. Phys. **5**, 57 (2003).
[28] R. Morgado, F. A. Oliveira, G. G. Batrouni, and A. Hansen, Phys. Rev. Lett. **89**, 100601 (2002).
[29] J. H. Thomas and N. O. Weiss, *Sunspots: Theory and Observations*, NATO Advanced Studies Institute, Series C: Mathematical and Physical Sciences Vol. 375 (Kluwer, Dordrecht, 1992).
[30] J. H. Thomas, N. O. Weiss, S. M. Tobias, and N. H. Brummell, Nature (London) **420**, 390 (2002).
[31] R. E. Rosensweig, J. Browaeys, J.-C. Bacri, A. Zebib, and R. Perzynski, Phys. Rev. Lett. **83**, 4904 (1999).